THE JOURNAL OF BIOLOGICAL CHEMISTRY VOL. 282, NO. 42, pp. 31028–31037, October 19, 2007


# Stereospecific Proton Transfer by a Mobile Catalyst in Mammalian Fructose-1,6-bisphosphate Aldolase*

Received for publication, June 15, 2007, and in revised form, August 13, 2007 Published, JBC Papers in Press, August 29, 2007, DOI 10.1074/jbc.M704968200

**Miguel St-Jean**[1] **and Jurgen Sygusch**[2]

*From the Department of Biochemistry, Université de Montréal, Montréal, Québec H3C 3J7, Canada*

**Class I fructose-1,6-bisphosphate aldolases catalyze the interconversion between the enamine and iminium covalent enzymatic intermediates by stereospecific exchange of the pro(*S*) proton of the dihydroxyacetone-phosphate C3 carbon, an obligatory reaction step during substrate cleavage. To investigate the mechanism of stereospecific proton exchange, high resolution crystal structures of native and a mutant $Lys^{146} \rightarrow$ Met aldolase were solved in complex with dihydroxyacetone phosphate. The structural analysis revealed trapping of the enamine intermediate at $Lys^{229}$ in native aldolase. Mutation of conserved active site residue $Lys^{146}$ to Met drastically decreased activity and enabled trapping of the putative iminium intermediate in the crystal structure showing active site attachment by C-terminal residues 360–363. Attachment positions the conserved C-terminal $Tyr^{363}$ hydroxyl within 2.9 Å of the C3 carbon in the iminium in an orientation consistent with incipient *re* face proton transfer. We propose a catalytic mechanism by which the mobile C-terminal $Tyr^{363}$ is activated by the iminium phosphate via a structurally conserved water molecule to yield a transient phenate, whose developing negative charge is stabilized by a $Lys^{146}$ positive charge, and which abstracts the C3 pro(*S*) proton forming the enamine. An identical C-terminal binding mode observed in the presence of phosphate in the native structure corroborates $Tyr^{363}$ interaction with $Lys^{146}$ and is consistent with transient C terminus binding in the enamine. The absence of charge stabilization and of a mobile C-terminal catalyst explains the extraordinary stability of enamine intermediates in transaldolases.**

Stereospecificity is one of the hallmarks of enzyme catalysis. Aldolases, which are abundant and ubiquitous enzymes, catalyze stereospecific carbon-carbon bond formation, one of the most important transformations in living organisms. Their role is best known in glycolysis where fructose-1,6-bis(phosphate) (FBP)[3] aldolases (EC 4.1.2.13) promote the cleavage of FBP to triose phosphates, D-glyceraldehyde-3-phosphate (G3P), and dihydroxyacetone phosphate (DHAP). A common feature to class I enzymes is the use of a covalent mechanism for catalysis implicating iminium (protonated Schiff base) formation between a lysine residue on the enzyme and a ketose substrate (1) that entails stereospecific proton exchange in the covalent intermediate (2). Of the three aldolase isozymes found in vertebrates (3), the catalytic mechanism has been extensively studied using class I aldolase A from rabbit muscle and key intermediates are depicted in reaction Scheme 1.

In the condensation direction, the reaction involves covalent intermediate formation with the keto triose phosphate DHAP followed by condensation with the aldehyde G3P to form the ketose of the acyclic FBP substrate (4, 5). To form the C3-C4 bond of FBP, the enzyme stereospecifically abstracts the pro(*S*) C3 proton of the trigonal iminium **1** (6, 7) that is formed from the Michaelis complex with DHAP thereby generating via the enamine **2** (2) the carbanionic character at C3 of DHAP for the aldol reaction. The nascent carbon-carbon bond has the same orientation as the pro(*S*) $\alpha$-hydrogen initially abstracted from the DHAP imine intermediate. The overall retention of configuration at C3 requires that proton abstraction from **1** to yield the enamine **2** and condensation with aldehyde in **3** must take place from the same direction on the enzyme (8). The iminium intermediate formed is then hydrolyzed and FBP is released by the inverse reaction sequence shown in Scheme 1.

A distinguishing mechanistic feature of class I aldolases is the relative stability of the iminium **1** and enamine **2** forms, which is a consequence of the catalytic requirements. The enzyme must stabilize the enamine **2** and/or the preceding iminium **1** such that no decomposition occurs prior to reaction with the aldehyde as shown in **3**. This stability is reflected in solution where the enzymatic populations **1** and **2** represent 20 and 60%, respectively, of bound DHAP on the muscle enzyme under equilibrium conditions (9). The interconversion between the two forms implicates the conserved C-terminal $Tyr^{363}$ residue whose proteolysis inhibits the stereospecific proton exchange step, making it rate-limiting (10), whereas the penultimate residues (357–362) of the C-terminal region modulate the rate of exchange reaction (11). The C-terminal region (residues 343–363) is conformationally mobile (12, 13), has an extended secondary structure (14, 15), and distinguishes mammalian aldo-

* This work was supported in part by the Natural Science and Engineering Research Council (Canada) and Canadian Institutes for Health Research. Work was carried out in part at the National Synchrotron Light Source, Brookhaven National Laboratory, which is supported by the United States Department of Energy, Division of Materials Sciences and Division of Chemical Sciences under contract DE-AC02-98CH10886. The costs of publication of this article were defrayed in part by the payment of page charges. This article must therefore be hereby marked "*advertisement*" in accordance with 18 U.S.C. Section 1734 solely to indicate this fact.

*The atomic coordinates and structure factors (code 2QUT, 2QUV, and 2QUU) have been deposited in the Protein Data Bank, Research Collaboratory for Structural Bioinformatics, Rutgers University, New Brunswick, NJ (http://www.rcsb.org/).*

[1] Recipient of a Ph.D. scholarship from the Fonds Québécois de la Recherche sur la Nature et les Technologies.

[2] To whom correspondence should be addressed: CP 6128, Station Centre Ville, Montréal, Quebec H3C 3J7, Canada. Tel.: 514-343-2389; Fax: 514-343-6463; E-mail: Jurgen.Sygusch@UMontreal.CA.

[3] The abbreviations used are: FBP, fructose-1,6-bis(phosphate); G3P, D-glyceraldehyde 3-phosphate; DHAP, dihydroxyacetone phosphate; WT, recombinant wild type; DERA, D-2-deoxyribose-5-phosphate aldolase.

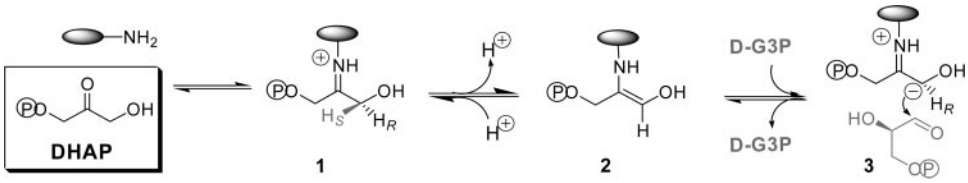


SCHEME 1. **Intermediates of the catalytic mechanism in class I aldolases.**

lases and their orthologues. Although a number of structural studies have been performed that have investigated intermediates in class I aldolases (15–18), characterization of the interconversion between the iminium and the enamine has so far proven elusive at the structural level.

To investigate the mechanism of stereoselective proton transfer in class I aldolases and how the enzyme is able to make efficient use of intermediates that are intrinsically unstable molecules, high resolution crystallographic studies were undertaken of rabbit muscle class I FBP aldolase in complex with DHAP using aldolase crystals incubated in the presence of DHAP in non-acidic buffer (pH 7.5), similar to kinetic studies (9). Flash freezing of a native rabbit muscle aldolase crystal soaked in a saturating DHAP solution trapped the enamine intermediate. On the other hand, a crystal of the active site mutant $Lys^{146} \rightarrow$ Met revealed DHAP bound as the iminium intermediate and interacting with the C-terminal tyrosine in the active site. Attachment by the C-terminal region yielded reaction geometry conducive for incipient proton transfer at the DHAP C3 carbon and explained proton exchange chirality.

## MATERIALS AND METHODS

*Purification and Crystallization*—Expression and purification of recombinant native (WT) and $Lys^{146} \rightarrow$ Met mutant (K146M) rabbit muscle aldolases were performed as described previously (11, 15, 19) and using *Escherichia coli* strain BL21 SI for overexpression of recombinant proteins (Invitrogen). Aldolase concentration was determined using an extinction coefficient of 0.91 $(mg/ml)^{-1}$ at 280 nm (20). WT and K146M aldolases were crystallized using the conditions reported previously (15).

*Proton Exchange*—Stereospecific pro(*S*) proton exchange at the C3 carbon of DHAP catalyzed by WT and K146M aldolases and WT aldolase crystals was followed by appearance of the tritium isotope label as (*S*)-[3-$^3H_1$]DHAP from tritiated water. Incorporation of the tritiated label at (*S*)-C3 of DHAP in the presence of $[^3H]H_2O$ was determined using an ion exchange protocol (Dowex $Cl^-$ resin) described in the literature (8). Carboxypeptidase A-treated aldolase was prepared according to conditions described previously (10). Digestion of aldolase by carboxypeptidase A was monitored by loss of enzymatic activity using a coupled assay and following NADH oxidation at 340 nm (21). The proteolyzed enzyme was separated from carboxypeptidase A by size exclusion chromatography when aldolase activity was decreased to 5% of the original activity.

*Data Collection and Processing*—WT aldolase crystals were soaked either for 2 min in ligand buffer containing DHAP (mother liquor plus 1 mM DHAP) or in phosphate buffer for 5 min (mother liquor plus 20 mM $NaH_2PO_4$). A K146M mutant aldolase crystal was soaked for 10 min in a ligand buffer containing a higher concentration of DHAP (mother liquor plus 20 mM DHAP). Prior to data collection, single crystals were cryoprotected in a soaking buffer containing 15% glycerol and immediately flash frozen in a stream of gaseous $N_2$ cooled to 100 K. Data collections were performed at beamline X8-C of the National Synchrotron Light Source (Brookhaven National Laboratory, Upton, NY) and diffracted intensities were measured using a Quantum4 charge-coupled device detector (Area Detector Systems, Poway, CA). All data sets were processed with HKL2000 (22) and the results are summarized in Table 1.

*Structure Determination and Refinement*—Liganded crystal structures were isomorphous with the crystal structure of native aldolase and belong to the monoclinic space group $P2_1$. Structures were solved by difference electron density maps using a native aldolase homotetramer structure as reference model (Protein Data Bank code 1ZAH) (15). Each asymmetric unit contains one homotetramer, consistent with the biologically active form of the enzyme. Refinement was performed using all reflections having an $I/\sigma(I) > 1$, however, electron density maps were calculated to the resolution indicated in the Table 1 to ensure at least ~70% completeness in the highest resolution shell with an $I/\sigma(I) > 2$. Each refinement cycle was performed as reported previously (15) using the Crystallography and NMR System (23) and O (24). The PRODRG server was used to generate ligand topology and parameter files (25). The presence of ligands in the final models was confirmed by observation of simulated annealing $F_o - F_c$ omit maps. Final model statistics, calculated with CNS and PROCHECK (26), are shown in Table 1. The coordinates and structure factors of WT aldolase soaked with DHAP, WT aldolase soaked with inorganic phosphate ($P_i$), and K146M aldolase soaked with DHAP have been deposited with the Protein Data Bank (codes 2QUT, 2QUV, and 2QUU, respectively). The final structure models have $R_{cryst}$ ($R_{free}$) values of 0.159 (0.191), 0.144 (0.191), and 0.157 (0.195), respectively. The corresponding positional errors in atomic coordinates using Luzzati plots were estimated at 0.17, 0.18, and 0.18 Å, respectively. Errors in hydrogen bond distances and positional differences are reported as standard deviations and were estimated based on their value in each subunit of the aldolase homotetramers unless specified otherwise. All figures were prepared using the program PyMOL (27). Superpositions were performed also with the program PyMOL overlaying Cα atom coordinates of aldolase residues 158–259 that are invariant to binding events as noted previously (15).

Chemical identity of covalent intermediates trapped in the WT-DHAP and K146M-DHAP structures was selected from simulated annealing $F_o - F_c$ omit maps using the real space statistic, $R_{fact}$, calculated in O (RS_FIT command). The statistic assesses the fit of $Lys^{229}$ Cε and Nζ atoms and DHAP C1, C2, C3, and O3 atoms in enamine and iminium forms to the electron density. In the enamine, $Lys^{229}$ Nζ would be $sp^3$ hybridized, whereas in the iminium, the hybridization would be $sp^2$. The discrimination of this difference in hybridization between the iminium and the enamine was quantified using a paired Student's *t* test comparing pairwise $R_{fact}$ statistics for identical

**TABLE 1**
**Data collection and refinement statistics**

| | WT-DHAP | WT-$P_i$ | K146M-DHAP |
|---|---|---|---|
| **Data collection** | | | |
| Resolution (Å) | 50-1.88 (1.98-1.88)[a] | 50-2.22 (2.34-2.22)[a] | 50-1.98 (2.07-1.98)[a] |
| Wavelength (Å) | 0.9795 | 0.9795 | 1.100 |
| Unique reflections/redundancy | 111,679/3.7 (14,586/3.1) | 67,988/3.6 (9,692/3.4) | 96,378/3.5 (9,641/2.5) |
| Completeness (%) | 98.5 (90.4) | 99.6 (99.8) | 96.5 (77.3) |
| Average $I/\sigma(I)$ | 15.2 (2.4) | 7.9 (2.4) | 21.4 (3.8) |
| $R_{sym}$[b] | 0.087 (0.466) | 0.146 (0.607) | 0.052 (0.258) |
| Space group | $P2_1$ | $P2_1$ | $P2_1$ |
| Unit cell parameters | | | |
| $a$ (Å), $b$ (Å), $c$ (Å), $\beta$ (°) | 82.8, 102.9, 84.2, 98.5 | 83.0, 102.7, 84.6, 98.2 | 83.9, 103.7, 84.9, 98.8 |
| **Refinement** | | | |
| Number of atoms | | | |
| Protein | 10,767 | 10,973 | 10,820 |
| Water | 2,860 | 2,592 | 2,230 |
| Hetero | 36 | 35 | 36 |
| $\sigma$ cutoff; $I/\sigma(I) >$ | 1 | 1 | 1 |
| $R_{cryst}$ (%)[c] | 15.9 | 14.4 | 15.7 |
| $R_{free}$ (%)[d] | 19.1 | 19.1 | 19.5 |
| Root mean square deviation | | | |
| Bond length (Å) | 0.005 | 0.006 | 0.005 |
| Bond angle (°) | 1.247 | 1.330 | 1.211 |
| Average $B$-factor (Å$^2$) | 28.8 | 28.6 | 25.1 |
| Ramachandran analysis[e] (%) | | | |
| Most favorable | 91.6 | 90.2 | 91.4 |
| Allowed | 8.4 | 9.8 | 8.6 |
| Luzzati positional error (Å) | 0.17 | 0.18 | 0.18 |

[a] All values in parentheses are given for the highest resolution shell.
[b] $R_{sym} = \Sigma_{hkl}\Sigma_i|I_i(hkl) - \bar{I}_i(hkl)|/\Sigma_{hkl}\Sigma_i I_i(hkl)$, with $i$ running over the number of independent observations of reflection $hkl$.
[c] $R_{cryst} = \Sigma_{hkl}||I_o(hkl)| - |I_c(hkl)||/\Sigma_{hkl}|I_o(hkl)|$.
[d] $R_{free} = \Sigma_{hkl\in T}||I_o(hkl)| - |I_c(hkl)||/\Sigma_{hkl\in T}|I_o(hkl)|$, where $T$ is a test data set randomly selected from the observed reflections prior to refinement. Test data set was not used throughout refinement and contains 5, 5, and 10% of the total unique reflections for WT-DHAP, WT-$P_i$, and K146M-DHAP, respectively.
[e] Analyzed by PROCHECK (26).

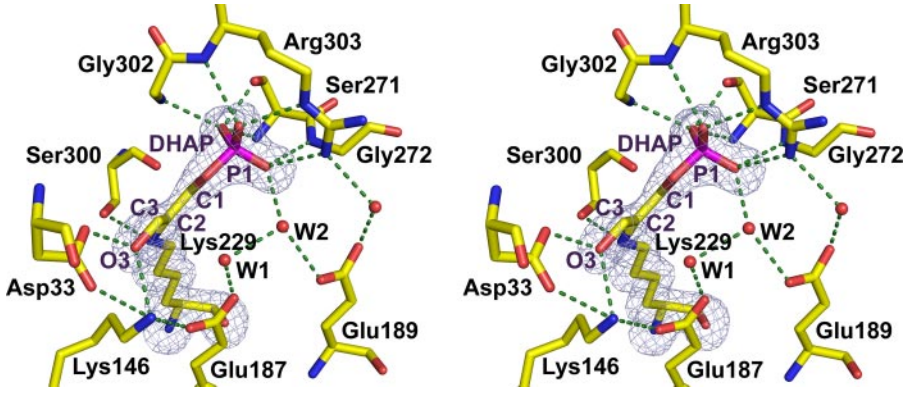


FIGURE 1. **Electron density showing the enamine intermediate trapped in the active site of rabbit muscle aldolase.** DHAP P1 phosphate is extensively bound making interactions with $Ser^{271}$, $Gly^{272}$, $Gly^{302}$, and $Arg^{303}$. DHAP C3 hydroxyl interacts with $Asp^{33}$ and $Lys^{146}$ stabilizing it in geometry coplanar with DHAP carbon atoms. Difference electron density was calculated from a 1.88-Å simulated annealing $F_o - F_c$ omit map encompassing $Lys^{229}$ and DHAP and contoured at 3.5$\sigma$. The same color scheme was used in all figures with *green dashes* to illustrate hydrogen bonding interactions and salt bridges, and *red spheres* to represent water molecules, unless stated otherwise.

subunits having the bound DHAP refined as either iminium or enamine form.

## RESULTS

*Enamine Intermediate*—Flash freezing of a WT aldolase crystal in the presence of DHAP trapped a covalent intermediate in each aldolase subunit. Continuous electron density, extending beyond $Lys^{229}$ N$\zeta$ in each subunit, shown in Fig. 1, indicates formation of a stable covalent adduct with DHAP. The planar shape of the electron density observed about the DHAP C2 carbon indicates trigonal hybridization, whereas non-planar shape of the electron density about the $Lys^{229}$ N$\zeta$ atom suggests tetrahedral hybridization and is consistent with trapping of a *cis*-enamine intermediate in each aldolase subunit (Fig. 2*A*). Comparison of average *B*-factors between bound DHAP and interacting side chains, 24 ± 3 and 21 ± 3 Å$^2$, respectively, indicates full active site occupancy by DHAP. To validate the electron density interpretation, real space $R_{fact}$ was evaluated (24) to objectively assess model fit to the electron density. The resulting paired Student's *t* test statistic calculated based on $R_{fact}$ values for DHAP modeled as either an enamine or an iminium was discriminatory with $p = 0.042$, the enamine having consistently lower $R_{fact}$ values in all subunits. This distinction is statistically significant and confirms trapping of a genuine enamine intermediate. Proton exchange in WT aldolase crystals as measured by production of (*S*)-[3-$^3H_1$]DHAP (Table 2) indicates 10 turnovers within the 2-min soaking period of DHAP into the aldolase crystal and corroborates equilibrium trapping of an enamine intermediate in all subunits. Coplanarity of DHAP C1, C2, C3, and O3 atoms, a requisite structural feature in the enamine intermediate, further supports identification of the intermediate as the enamine.

Numerous interactions with active site residues stabilize the covalent intermediate, as shown in Fig. 1. These interactions

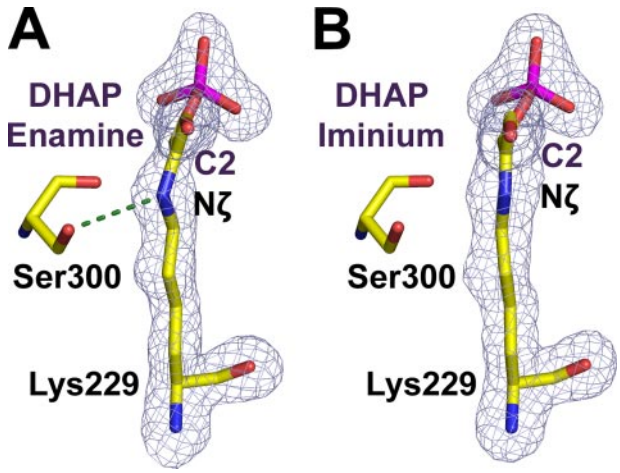


FIGURE 2. **Discrimination of enzymatic intermediates formed with DHAP in aldolase active site.** Geometry of enzymatic intermediates was used to identify the chemical entity of the trapped DHAP-aldolase complexes. *A*, an enamine intermediate was identified in all subunits in the structure of native aldolase on the basis of $sp^3$ hybridization of $Lys^{229}$ Nζ and enables hydrogen bond formation between the $Ser^{300}$ hydroxyl and $Lys^{229}$ Nζ. Difference electron density shown was calculated as described in the legend to Fig. 1 and contoured at 4.0σ. *B*, an iminium intermediate was identified in all subunits in the structure of the K146M mutant aldolase complexed with DHAP. $sp^2$ hybridization of $Lys^{229}$ Nζ precludes hydrogen bond formation with $Ser^{300}$. Difference electron density was calculated from a 1.98-Å simulated annealing $F_o - F_c$ omit map encompassing $Lys^{229}$ and DHAP and contoured at 4.0σ.

**TABLE 2**

**Stereospecific pro(*S*) proton exchange at C3 of DHAP**

The rate of proton exchange was measured by appearance of tritium isotope label as (*S*)-[3-$^3H_1$]DHAP from tritiated water as described under "Materials and Methods."

| Aldolase | $^1H/^3H$ exchange rate[a] |
|---|---|
| | $min^{-1}$ |
| Native | $9.7 \times 10^2 \pm 1.3 \times 10^2$ |
| Native crystals[b] | $5.14 \pm 0.69$ |
| K146M | $0.0733 \pm 0.0086$ |
| Carboxypeptidase-treated aldolase | $0.457 \pm 0.061$ |
| Background[c] | $0.0118 \pm 0.0011$ |

[a] Error calculated using individual errors derived at each step of the measurement protocol.
[b] Size of crystals used was comparable to crystals used for data collection.
[c] Exchange rate measured in the absence of aldolase.

are identical to those reported in the structure of the iminium intermediate formed with FBP substrate by the same enzyme (15) including an unusual short hydrogen bond (2.4 ± 0.1 Å) with $Ser^{271}$ side chain. $Asp^{33}$ and $Lys^{146}$ further stabilize the intermediate by hydrogen bonding with DHAP C3 hydroxyl and on the basis of consistency with the hydrogen bonding pattern, $Lys^{146}$ is protonated. An additional hydrogen bond between $Ser^{300}$ hydroxyl and $Lys^{229}$ Nζ specifically stabilizes the enamine intermediate (Fig. 2*A*), which is not possible in the carbanion or the iminium requiring $sp^2$ hybridization at $Lys^{229}$ Nζ. Stabilization of the enamine by the hydrogen bond is reflected in the reduced pro(*S*) proton exchange rate at C3 of DHAP when measured for mutations $Ser^{300}$ to Ala and Cys and compared with native enzyme (28). Elimination of hydrogen bonding potential in mutation S300A yielded a 5-fold reduction in exchange rate, whereas weakening the same hydrogen bond in mutation S300C reduced the rate 3-fold.

Active site binding of DHAP induces identical conformational changes in each aldolase subunit with respect to native enzyme that results in the asymmetric narrowing of the active site cleft, similar to the conformational change observed in the structure of the iminium intermediate formed with FBP (15). From Table 3, conformational displacements of these helical regions, although smaller than for the FBP bound structure, are significant when compared with residues 158–259 of the β-barrel, which make up part of the active site and inter-subunit contacts.

**TABLE 3**

**Conformational changes induced by DHAP binding**

Conformational changes were identified on the basis of differences between identical atomic positions in liganded aldolases as compared with native enzyme. Comparisons were made between the same subunits and then averaged over all subunits in the aldolase tetramer. Values tabulated represent root mean square differences between equivalent Cα atoms and are given in Å.

| Residues selected | WT-DHAP | WT-FBP[a] |
|---|---|---|
| 158–259 | 0.09 | 0.09 |
| 33–65[b] | 0.72 | 1.02 |
| 302–329[b] | 0.66 | 0.84 |
| 35[b] | 0.66 | 1.25 |
| 38[b] | 0.30 | 0.62 |
| 303[b] | 0.70 | 0.74 |

[a] Protein Data Bank code 1ZAI (15).
[b] Calculation of root mean square differences for these residues was based on superposition of liganded complexes onto native enzyme using Cα atom coordinates of residues 158–259.

Superposition of the native and enamine-bound structures identified two conserved water molecules, W1 and W2, whose positions remain invariant upon DHAP attachment (Fig. 1). W1 that has a low *B*-factor (23 ± 4 $Å^2$), similar to that of Cα atoms of residues 10–343 (20 ± 8 $Å^2$), is positioned by hydrogen bonds with $Glu^{187}$ and W2, at 3.1 ± 0.1 Å from both DHAP C2 and C3 carbons. The orientation of W1 is perpendicular to the enamine plane and more in line with the DHAP C2 carbon. A similar in line geometry with the C3 carbon position would require only a slight positional displacement by the water molecule.

*Phosphate Binding*—Phosphate anion binding to aldolase is inhibited by DHAP (29) indicating competition for the P1 phosphate binding site. To address the specificity of the induced conformational changes in stabilization of the enamine intermediate, a WT aldolase crystal was soaked in a phosphate buffer. Structural analysis revealed subunit heterogeneity in response to phosphate binding with respect to the extent of asymmetric narrowing of the active site cleft and binding specificity was controlled by active site attachment of C-terminal residues 360–363.

In one subunit (D), phosphate anion binding coincides with the DHAP P1 phosphate site in the enamine structure and concomitant with the C terminus occluding the active site (Fig. 3). The conformational changes induced by phosphate bound at the P1 phosphate binding site were greatest in this subunit and comparable with those induced by DHAP with respect to the native enzyme. In addition, $Ser^{38}$ from the helical region 33–65 was displaced by 0.6 Å along the helical axis to avoid close contact with $Tyr^{363}$ in the active site. An additional partially occupied phosphate binding site was found at the subunit interface and interacting with residues $Gln^{202}$, $Arg^{258}$, and $Lys^{12}$, the latter from an adjacent subunit.

In two other subunits (A and C), the phosphate anion binding site is shifted ~2 Å from the previous DHAP P1 phosphate binding locus toward the surface of the active site (not shown).

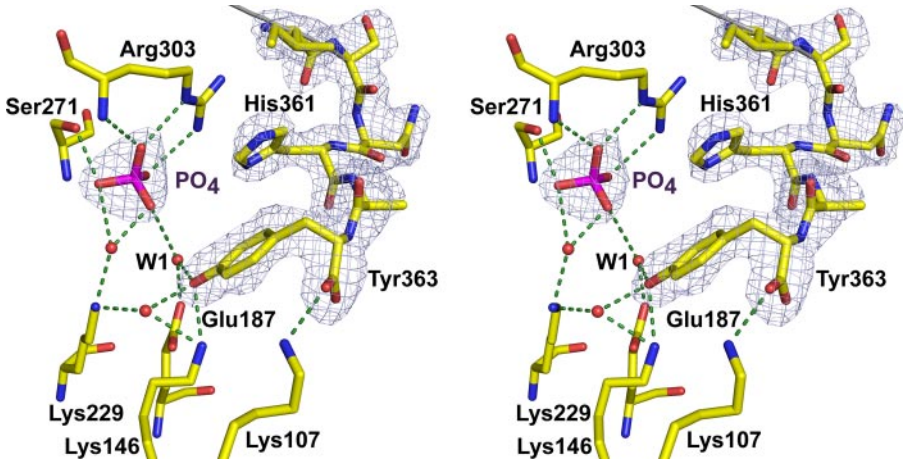


FIGURE 3. **Active site attachment by the phosphate anion at the DHAP P1 binding locus recruits its proper C-terminal region.** C-terminal Tyr$^{363}$ interacts with Lys$^{107}$, Lys$^{146}$, and active site water molecules, whereas His$^{361}$ stacks with Arg$^{303}$ that binds the phosphate anion as shown in Fig. 1. Difference electron density was calculated from a 2.22-Å simulated annealing $F_o - F_c$ omit map encompassing C-terminal residues 358–363 and phosphate anion and contoured at 3.5$\sigma$.

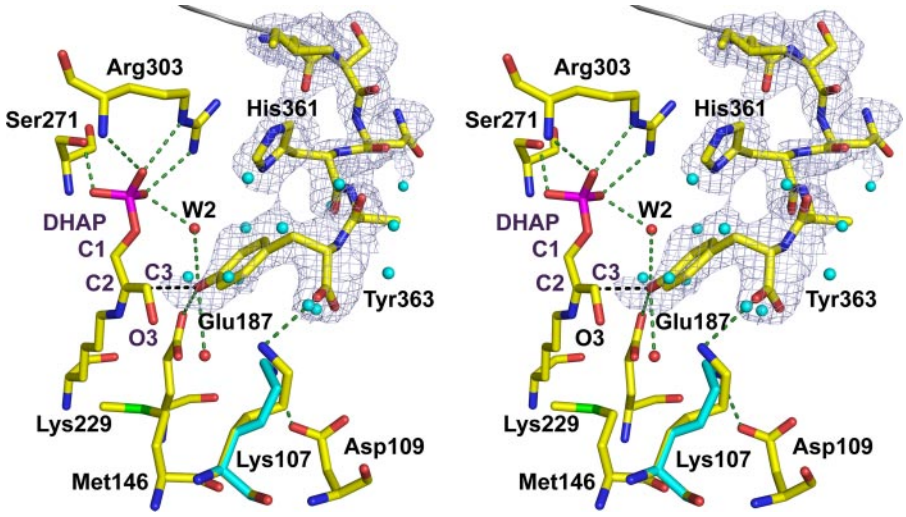


FIGURE 4. **C terminus binding upon iminium formation in the active site of a subunit of the K146M mutant aldolase.** The bound C terminus is shown superposed onto an alternate conformation of water molecules (*cyan spheres*) and Lys$^{107}$ side chain (*cyan*). Occupancy of C-terminal residues 360–363 was refined to 0.5 with water molecules accounting for the remaining electron density shown. Notably, the Tyr$^{363}$ hydroxyl is positioned at 2.9 Å from the DHAP C3 and in an orientation that would favor the stereospecific pro(*S*) $\alpha$-proton abstraction of the iminium (*black dashes*). Tyr$^{363}$ carboxylate binds Lys$^{107}$ whose side chain conformation is identical to that observed in native structures. Difference electron density was calculated from a 1.98-Å simulated annealing $F_o - F_c$ omit map encompassing C-terminal residues 358–363 and contoured at 2.5$\sigma$.

Binding at this site does not involve active site attachment by the C terminus region nor significant conformational changes and is of lower affinity as phosphate positions refined to partial occupancy. The C-terminal regions are fully bound at their proper subunit interface as in the enamine structure and C terminus Tyr$^{363}$ interacts with the same residues involved in phosphate binding as those implicated at the subunit interface of D.

In the remaining subunit (B), electron density in the active site was interpreted as a superposition of the two previous mutually exclusive phosphate binding sites, which included alternate geometries of the C-terminal regions, consistent with the refined partial occupancy for each site. Increased C terminus resistance to carboxypeptidase A degradation in the presence of phosphate (12) would argue that physiological concentrations of phosphate enhance active site sequestration of Tyr$^{363}$, as observed in subunits B and D.

*Iminium Intermediate*—Site-directed mutation of Lys$^{146}$ to Met severely compromises aldolase catalytic activity (30) and stereospecific proton exchange at the enamine, shown in Table 2. Flash freezing of a K146M mutant crystal soaked in the presence of DHAP trapped a covalent intermediate in the active site of all subunits. The fit by DHAP to the electron density, shown in Fig. 2*B*, and modeled as an iminium instead of an enamine was statistically significant yielding a paired Student's *t* test statistic of $p = 0.035$. Comparison of average *B*-factors between bound DHAP and interacting side chains, 23 ± 2 and 23 ± 3 Å$^2$, respectively, suggests full active site occupancy by DHAP. Covalent attachment by DHAP yielded a conformation including coplanarity of Lys$^{229}$ N$\zeta$, DHAP C1, C2, C3, and O3 atoms as well as an unusual short hydrogen bond (2.3 ± 0.1 Å) with the Ser$^{271}$ side chain. Phosphate anion was bound at the same loci in a K146M-$P_i$ structure compared with the WT-$P_i$ structure,[4] indicating that the mutation does not affect active site integrity with respect to ligand binding at the P1 phosphate binding site.

Surprisingly, in subunit D of the K146M-DHAP structure, the last four residues of the C-terminal region, disordered in the native and enamine structures, were bound ordered in the active site with Tyr$^{363}$ adjacent to the iminium intermediate (Fig. 4). Conformational similarity of the bound C-terminal region with that of the same C-terminal region observed in WT-$P_i$ (Fig. 3) (root mean square deviation of 0.51 Å for backbone atoms of residues 360–363) suggests that the observed C-terminal conformation is determined through contacts with active site residues, shown in Fig. 4, that are conserved (31). Lys$^{107}$ displays two conformations of equal occupancy, one of which interacts with the Tyr$^{363}$ carboxylate, also observed in the WT-$P_i$ structure, whereas in the second conformation, Lys$^{107}$ makes a salt bridge with Asp$^{109}$ present in all subunits.

Active site interaction positions the Tyr$^{363}$ hydroxyl 2.9 Å from the DHAP C3 carbon and approximately perpendicular to

[4] M. St-Jean and J. Sygusch, unpublished data.

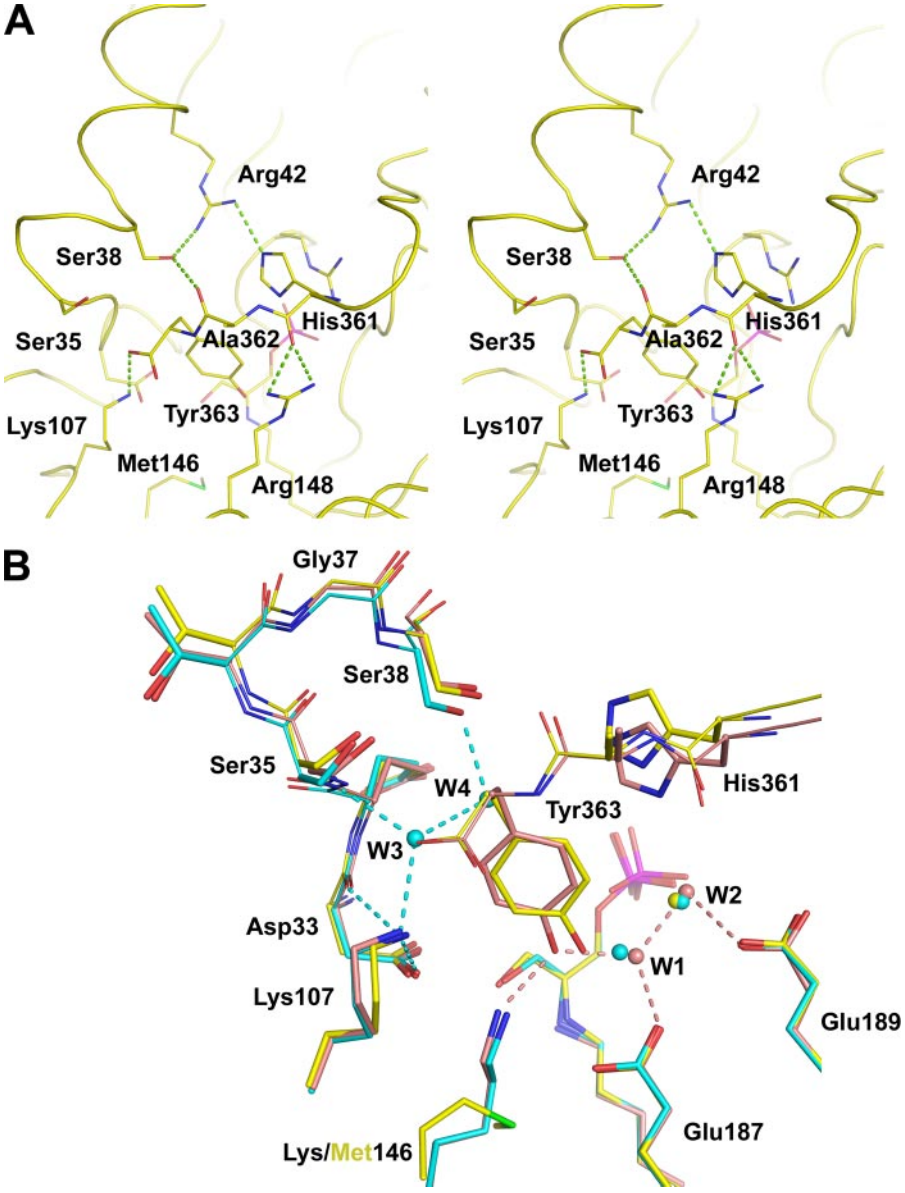


FIGURE 5. **Interactions made by the C-terminal region in the active site of muscle aldolase.** *A*, C-terminal residues 361–363 interact with Ser[38], Arg[42], Lys[107], and Arg[148] in the active site of the K146M-DHAP structure. *B*, superposition of WT-DHAP (*cyan*), K146M-DHAP (*yellow*), and WT-$P_i$ (*pink*) structures. In the WT-DHAP structure, Ser[38] interacts with Lys[107] via two bridging water molecules, W3 and W4. Active site entry by the C terminus in K146M-DHAP and WT-$P_i$ structures displaces W3 and W4. Outwards movement of the flanking helix (residues 33–45) along its helical axis precludes a close contact that would result between Ser[38] side chain and Tyr[363] C$\beta$ upon active site binding.

the *re* face of the plane as defined by DHAP carbon atoms. Active site attachment by the C terminus was not an artifact of the Lys[146] → Met mutation, as C terminus binding was not observed in the active site of unbound K146M mutant aldolase.[4] DHAP binding induced the same conformational changes in both $\alpha$-helical regions as in the enamine although displacements of the helices comprising residues 33–65 were comparatively smaller (<0.4 Å) in all subunits of the K146M mutant. The smaller displacement could be reasonably explained by the loss of the interaction between Lys[107] and Asp[33] that anchors the flanking helix comprising residues 33–45.

*C-terminal Active Site Docking*—To discern conformational changes corresponding to entry of the C terminus into the active site, the structures of WT-DHAP, K146M-DHAP, and WT-$P_i$ were compared after superposition onto the native structure. Two conformational states were evident for each aldolase subunit and are a function of the C-terminal conformation: an open conformation, observed in the WT-DHAP structure, where the C terminus is not bound in the active site and a closed conformation, observed in subunit D of the WT-$P_i$ and K146M-DHAP structures (Figs. 3 and 4, respectively), where the C-terminal region binds the active site. C-terminal active site interactions include Tyr[363] carboxylate salt bridging with Lys[107] and hydrogen bonding linking Ala[362] backbone carbonyl with Ser[38] and His[361] with Arg[42], which in turn interacts with Ser[38] (Fig. 5*A*). The Arg[148] side chain further stabilizes attachment by hydrogen bonding with the His[361] backbone carbonyl. In the closed conformation, the helix flanking the active site (residues 33–45) and interacting with the C-terminal region not only narrows the active site cleft but also shifts by ~0.5 Å outwards along its helical axis relative to the structure of the enamine.

The outward positional movement of the flanking helix disrupts a hydrogen bonding network mediated by two water molecules that involves Ser[38]. The network in the open conformation entails Lys[107] N$\zeta$ hydrogen bonding both with Asp[33] side chain and backbone carbonyl and with a water molecule W3. W3 in turn hydrogen bonds Ser[35] backbone amide and another water molecule W4, which in turn hydrogen bonds Ser[38] hydroxyl (Fig. 5*B*). C terminus entry displaces W3 and W4 and concomitant movement of the flanking helix enables Ser[38] to interact with the incoming C-terminal Ala[362] backbone carbonyl. Displacement by Ser[38] of the flanking helix is essential to avoid an otherwise close contact (2.6 Å) with Tyr[363] C$\beta$ (Fig. 5*B*). The hydrogen bond between Tyr[363] and Lys[146] (2.7 Å) in the WT-$P_i$ structure would result in a close contact of ~2 Å between the Tyr[363] hydroxyl and DHAP C3 carbon when superimposed onto the enamine structure (Fig. 5*B*). The close contact is alleviated in the iminium structure by slight lateral adjustment of Tyr[363] and His[361] side chains. Active site penetration by the Tyr[363] hydroxyl in the iminium displaces the

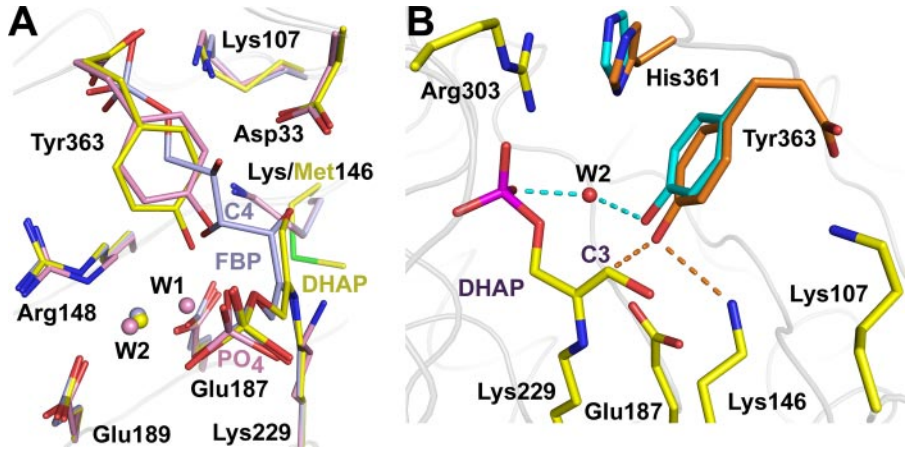


FIGURE 6. **Proposed mechanism for stereospecific proton transfer with conservation of reaction chirality.** *A*, superposition of WT-FBP (PDB code 1ZAI) (*light blue*), K146M-DHAP (*yellow*), and WT-$P_i$ (*pink*) structures shows active site binding by the C-terminal $Tyr^{363}$ at the same locus as the nascent G3P moiety of the iminium formed with FBP in aldolase. The close contact by $Tyr^{363}$ hydroxyl with the FBP C4 atom indicates that stereospecific proton transfer occurs in the same direction as G3P addition to the enamine. *B*, C-terminal $Tyr^{363}$ hydroxyl is activated by a catalytic mechanism implicating a proton transfer relay mediated by the DHAP P1 dianion via water molecule W2 (*cyan*). Subsequent small oscillation of the $Tyr^{363}$ side chain allows $Lys^{146}$ to electrostatically stabilize the developing negative charge on $Tyr^{363}$ (*orange*). In this configuration, $Tyr^{363}$ phenate is aligned to catalyze stereospecific transfer of the pro(*S*) $\alpha$-proton at DHAP C3 carbon.

conserved water molecule W1, bound by $Glu^{187}$, present in all subunits of WT-DHAP and WT-$P_i$ structures.

## DISCUSSION

The ability to cryotrap the enamine and iminium intermediates of the aldolase catalytic cycle in the crystalline state provided a unique opportunity to characterize conformational states associated with proton transfer during iminium-enamine interconversion. Analysis of the conformational states enabled a detailed description of the molecular events catalyzing stereospecific proton exchange by the C-terminal region in class I aldolases.

*DHAP Covalent Intermediates*—The covalent enzymatic complexes trapped in the presence of DHAP in crystals of native and K146M mutant rabbit muscle aldolases represent authentic enamine and iminium intermediates, respectively. A unique feature of the enamine structure is $Ser^{300}$ hydroxyl hydrogen bonding $Lys^{229}$ N$\zeta$ that is only possible in the enamine form and not in the iminium (Fig. 2). Stabilization of the enamine intermediate is further assisted by $Asp^{33}$ and $Lys^{146}$, which hydrogen bond DHAP O3 and maintain the DHAP O3 coplanar with respect to the C2 and C3 carbons that is requisite for resonance stabilization of the enamine form. The unusual short hydrogen bond between $Ser^{271}$ and the DHAP P1 phosphate in both iminium and enamine is not present in the case of the phosphate anion bound. Covalent attachment by DHAP apparently induces strain, which is resolved by short strong hydrogen bond formation (32).

*C-terminal Region*—The trapping of the C terminus in the active site of the K146M mutant, shown in Fig. 4, is the first structural evidence corroborating that C-terminal $Tyr^{363}$ engages in stereospecific proton exchange in rabbit muscle aldolase (10). Artifactual active site binding as a result of the mutation is unlikely as an identical interaction with active site residues is observed in the WT-$P_i$ structure. Partial occupancy by the C-terminal region in the mutant iminium intermediate indicates that the entropic penalty due to C-terminal ordering upon binding is compensated by binding interactions with active site residues and entropic gain due to displacement of water molecules, W3 and W4.

Comparison of the two DHAP bound structures indicates that in the enamine diminished active site hydrophobicity and electrostatic charge destabilization of $Lys^{107}$ by $Lys^{146}$, weakening $Lys^{107}$ interaction with the $Tyr^{363}$ carboxylate would diminish the active site interaction energy of $Tyr^{363}$. Reduced interaction energy would favor transient C-terminal attachment that is in agreement with the absence of C-terminal binding in the native enamine structure. Conformational mobility by the C-terminal region is requisite for its catalytic function, as in the closed conformation the C terminus would collide with the nascent G3P moiety of the FBP molecule, as seen in Fig. 6*A*. Weak interaction by the C-terminal region would thus limit its active site competition enabling product release and/or substrate binding. The extensive configurational entropy of the C-terminal region and its limited active site affinity are indispensable mechanistic requirements wherein the C-terminal region functions as a mobile catalyst.

Interactions made by the C-terminal region with active site residues are predominantly through its peptide backbone alluding to similar modes of active site docking by C-terminal regions of class I aldolase orthologues. The five penultimate residues of the C-terminal sequence are not conserved and only $Asn^{360}$ and $His^{361}$ side chains interact with the active site locus contacting side chains of residues, $Lys^{152}$ and conserved $Arg^{42}$, respectively. The flexible side chains of the interacting residues tolerate amino acid substitution obviating sequence conservation of the penultimate residues with regards to catalytic function. Differences in active site binding affinity due to sequence variation at residues 360 and 361 is consistent with modulation of the DHAP exchange reaction by chimeric constructs implicating these penultimate residues of the C-terminal region in aldolase orthologues (11).

*Stereospecific Proton Transfer*—The crystallographic structures are consistent with $Tyr^{363}$ facilitating the *re* face stereospecific pro(*S*) proton exchange with respect to the DHAP C3 carbon atom in the iminium and enamine intermediates of rabbit muscle aldolase. The immediate microenvironment of $Tyr^{363}$ in the active site is not hydrophobic consisting of charged residues and a water molecule that would argue for a solution $pK_a \sim 10.5$ for $Tyr^{363}$ and is supported by a proposed $pK_a > 9$ for the basic group involved in $\alpha$-proton abstraction in muscle aldolase (33). A $pK_a \sim 18$ has been estimated for the ionization at DHAP C3 (34), which in the iminium would be

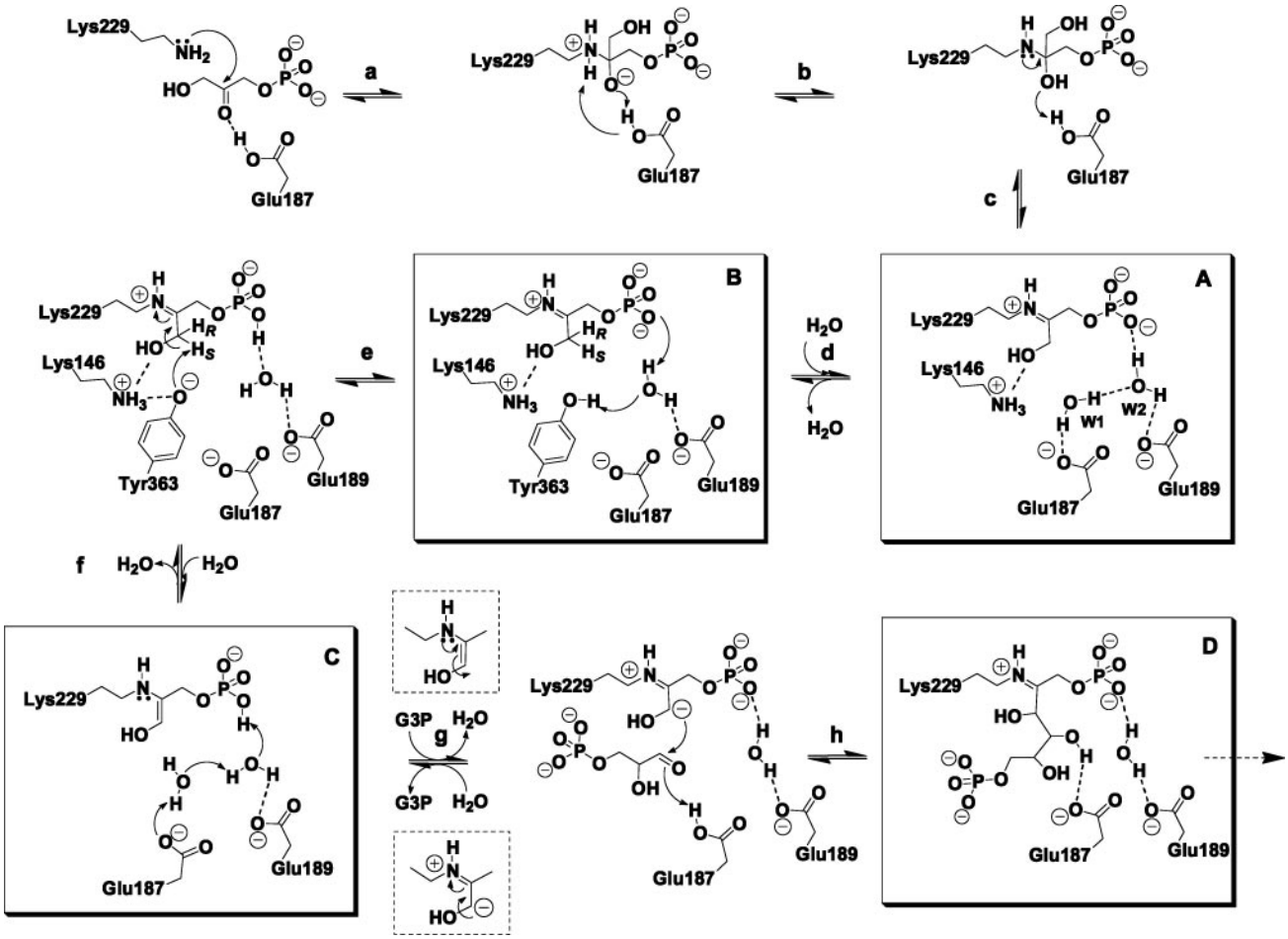


SCHEME 2. **FBP condensation in class I aldolase.**

lowered to a value approaching that of a tyrosine (35–37), favoring proton transfer by matching p$K_a$ values. Overlay of the K146M-DHAP and WT-$P_i$ structures onto the WT-FBP structure (15) positions the C terminus $Tyr^{363}$ hydroxyl in close contact with the C4 atom of the FBP molecule (Fig. 6*A*), indicating a common stereochemical route to bond formation at C3 in the proton exchange and G3P addition and corroborating overall retention of configuration at C3 in the enamine (8). A catalytic mechanism is outlined in Scheme 2 integrating the enzymological and crystallographic data and describing FBP condensation in class I FBP aldolases, including interconversion between the iminium and enamine forms.

The catalytic cycle begins by DHAP binding narrowing the active site cleft to stabilize ligand attachment. $Glu^{187}$ catalyzes iminium formation as previously described (15), shown in Scheme 2, reactions *a*–*c*. The resultant iminium, *panel A*, can be reversibly hydrolyzed by the conserved water molecule W1, activated by $Glu^{187}$ and is positioned perpendicular to the plane defined by DHAP carbon atoms and $Lys^{229}$ N$\zeta$ and hydrogen bonds the DHAP C2 carbon of the iminium, reaction *c*. Transient binding by $Tyr^{363}$, reaction *d*, displaces W1 in *panel B*, and $Tyr^{363}$ hydroxyl is activated by sequential proton transfer through the conserved water molecule W2, hydrogen bonded to the iminium phosphate dianion that acts as a conjugate base, reaction *e*. Proton abstraction generates the $Tyr^{363}$ phenate that is electrostatically stabilized by $Lys^{146}$, consistent with $Tyr^{363}$-$Lys^{146}$ interaction in the WT-$P_i$ structure; subsequent stereospecific pro(*S*) $\alpha$-proton abstraction by $Tyr^{363}$ phenate in reaction *f* generates the enamine, *panel C*. C terminus expulsion is followed by rebinding of water molecule W1. The enamine phosphate catalyzes proton transfer via intervening water molecules, W1 and W2, to generate the acid form of $Glu^{187}$ for subsequent aldehyde activation in reaction *g*. Concomitant attachment of G3P displaces W1 and the electrophilic character at C1 of the activated G3P aldehyde promotes carbanion mesomer formation. The acid form of $Glu^{187}$ thus catalyzes C–C bond formation, shown in reaction *h*, yielding the FBP iminium in *panel D*, described previously (15).

Proton transfer during the catalytic cycle is consistent with a trajectory of least atomic motion, including interconversion of the iminium to the enamine that entails only slight torsional librations by the $Tyr^{363}$ side chain in the active site, Scheme 2, reaction *e*, illustrated in Fig. 6*B*. Central to the proposed interconversion mechanism is the activation of the $Tyr^{363}$ hydroxyl. $Glu^{187}$ has been implicated in multiple proton transfers in the catalytic mechanism of the aldolase (15, 38) and as a conjugate base, $Glu^{187}$ could abstract the proton of the $Tyr^{363}$ hydroxyl. However, this possibility is unlikely as it would require deeper penetration of the $Tyr^{363}$ hydroxyl into the active site for proper hydrogen bonding with $Glu^{187}$, which is not observed. By con-

trast, the trajectory of the $Tyr^{363}$ hydroxyl resulting from a small side chain libration (~20°) primarily by the tyrosyl ring about its C$\alpha$–C$\beta$ bond (coupled to a similar movement by $His^{361}$ side chain) enables close contact (≤2.5 Å) with the invariant water molecule W2, hydrogen bonded to the DHAP P1 phosphate, or with DHAP C3 atom (Fig. 6*B*); the latter conformation also resulting in hydrogen bond formation with $Lys^{146}$ and thus electrostatically stabilizing the $Tyr^{363}$ phenate. The P1 phosphate dianion p$K_a$ ~ 6.45 (39) supports the role of the phosphate oxyanion as the conjugate base at physiological pH catalyzing proton transfer relayed through the invariant water molecule W2. The proposed mechanism explains the absence of $\alpha$-proton exchange in the presence of dihydroxyacetone sulfate, binding resulting in iminium but not enamine formation (40) as the sulfate dianion is too weakly basic to catalyze proton exchange. Indeed in model systems, the phosphate dianion has been shown to catalyze intramolecular $\alpha$-proton abstraction, whereas the sulfate dianion did not accomplish the same function (41).

The catalytic model reconciles longstanding findings implicating the C terminus in class I aldolase catalysis (10, 42). The 500-fold rate reduction upon $Tyr^{363}$ loss by proteolysis (43) is consistent with water molecule W1, activated by $Glu^{187}$ shown in *panel A*, partitioning between iminium hydrolysis and, to a lesser extend, pro(*S*) $\alpha$-proton abstraction. The activated water molecule is well aligned for nucleophilic attack at the DHAP C2 carbon, whereas a slight lateral shift (<1 Å) toward the DHAP C3 carbon would result in hydrogen bonding with $Lys^{146}$ and position it to catalyze the pro(*S*) $\alpha$-proton transfer. Electrostatic stabilization of a hydroxyl nucleophile by $Lys^{146}$, and indirectly $Lys^{107}$, would further facilitate alignment of the nucleophile for $\alpha$-proton transfer and predicts a pH dependence of enamine formation dependent on the respective p$K_a$ values of lysine residues. Indeed, pH profile analysis of enamine formation in the proteolyzed enzyme shows a sharp fall in DHAP trapped as enamine from pH 7.5 to 8.5, and was shown to depend on a change of approximately two protons with similar p$K_a$ values of ~8.0 (33).

*Mobile C-terminal Catalyst*—The C-terminal tyrosine is conserved in all class I FBP aldolases sequenced to date including orthologues found in mammals, higher plants, as well as parasites (31). Although proteolysis of the C-terminal region inhibits $\alpha$-proton exchange in the enamine, the enzyme retains transaldolase activity as proteolysis does not significantly affect the ability to exchange FBP with G3P (10, 44). Transaldolases that have the same fold and similar active site disposition of catalytic residues as class I aldolases (16) differ by the exceptional stability of their enamine (45) due to an absence of a mechanistic pathway enabling interconversion of the enamine to the iminium. Indeed, in contrast to class I aldolase, the active site of bacterial transaldolase B has no amino acid residue capable of charge stabilization vicinal to the C3 carbon of dihydroxyacetone and the enzyme lacks a mobile C-terminal region capable of mediating $\alpha$-proton transfer (46).

In the proton exchange mechanism describing interconversion of the acetaldehyde iminium to enamine in D-2-deoxyribose-5-phosphate aldolase (DERA), a water molecule that is activated by $Lys^{201}$, adjacent to the iminium forming $Lys^{167}$, was postulated on the basis of molecular mechanics as responsible for stereospecific pro(*S*) $\alpha$-protonation of the acetaldehyde C2 carbon (18). The water molecule is positioned competent for catalyzing proton transfer at the C2 position in the enamine and would, as in class I FBP aldolase, enable iminium hydrolysis at the C1 position, yet cleavage activity of native DERA exceeds that of carboxypeptidase-treated muscle aldolase by more than 400-fold. DERA, similar to muscle aldolase, also has a C-terminal region and mutation of its C terminus $Tyr^{259}$ to Phe diminishes catalytic activity by 200-fold (18). Even though the last eight residues of the C-terminal region in DERA are apparently conformationally disordered, molecular modeling indicates that the C terminus $Tyr^{259}$ can reach into the active site (18). Active site penetration by C terminus $Tyr^{259}$ to promote $\alpha$-proton exchange during iminium-enamine interconversion, as in muscle aldolase, would resolve the apparent mechanistic conflict of the same water molecule participating in two competing reactions. Finally, it is intriguing that in archaeal FBP aldolases, which do not have a mobile C terminus tyrosine catalyst, the cleavage reaction rate is 2 orders of magnitude lower compared with mammalian FBP aldolases (47).

*Acknowledgments—We thank Christine Munger for proton exchange experiments with the $Ser^{300}$ aldolase mutants and Drs. Casimir Blonski and Tina Izard for insightful critiques and suggestions. Assistance by Dr. L. Flaks, X8-C beamline, was appreciated. We also thank computational resources available at ASDP web site (asdp.bnl.gov).*

## REFERENCES

1. Grazi, E., Rowley, P. T., Chang, T., Tchola, O., and Horecker, B. L. (1962) *Biochem. Biophys. Res. Commun.* **9,** 38–43
2. Rose, I. A., and Rieder, S. V. (1958) *J. Biol. Chem.* **231,** 315–329
3. Penhoet, E. E., and Rutter, W. J. (1971) *J. Biol. Chem.* **246,** 318–323
4. Rose, I. A., and Warms, J. V. (1985) *Biochemistry* **24,** 3952–3957
5. Ray, B. D., Harper, E. T., and Fife, W. K. (1983) *J. Am. Chem. Soc.* **105,** 3731–3732
6. Jencks, W. P. (1969) *Catalysis in Chemistry and Enzymology*, pp. 120–121, McGraw-Hill Book Co., New York
7. Grazi, E., Cheng, T., and Horecker, B. L. (1962) *Biochem. Biophys. Res. Commun.* **7,** 250–253
8. Rose, I. A. (1958) *J. Am. Chem. Soc.* **80,** 5835–5836
9. Rose, I. A., Warms, J. V., and Kuo, D. J. (1987) *J. Biol. Chem.* **262,** 692–701
10. Rose, I. A., O'Connell, E. L., and Mehler, A. H. (1965) *J. Biol. Chem.* **240,** 1758–1765
11. Berthiaume, L., Tolan, D. R., and Sygusch, J. (1993) *J. Biol. Chem.* **268,** 10826–10835
12. Adelman, R. C., Morse, D. E., Chan, W., and Horecker, B. L. (1968) *Arch. Biochem. Biophys.* **126,** 343–352
13. Sygusch, J., Beaudy, D., and Allaire, M. (1990) *Arch. Biochem. Biophys.* **283,** 227–233
14. Blom, N., and Sygusch, J. (1997) *Nat. Struct. Biol.* **4,** 36–39
15. St-Jean, M., Lafrance-Vanasse, J., Liotard, B., and Sygusch, J. (2005) *J. Biol. Chem.* **280,** 27262–27270
16. Choi, K. H., Shi, J., Hopkins, C. E., Tolan, D. R., and Allen, K. N. (2001) *Biochemistry* **40,** 13868–13875
17. Lorentzen, E., Pohl, E., Zwart, P., Stark, A., Russell, R. B., Knura, T., Hensel, R., and Siebers, B. (2003) *J. Biol. Chem.* **278,** 47253–47260
18. Heine, A., DeSantis, G., Luz, J. G., Mitchell, M., Wong, C. H., and Wilson, I. A. (2001) *Science* **294,** 369–374
19. Morris, A. J., and Tolan, D. R. (1993) *J. Biol. Chem.* **268,** 1095–1100
20. Baranowski, T., and Niederland, T. R. (1949) *J. Biol. Chem.* **180,** 543–551
21. Racker, E. (1947) *J. Biol. Chem.* **167,** 843–854

22. Otwinowski, Z., and Minor, W. (1997) *Methods Enzymol.* **276,** 307–326
23. Brunger, A. T., Adams, P. D., Clore, G. M., DeLano, W. L., Gros, P., Grosse-Kunstleve, R. W., Jiang, J.-S., Kuszewski, J., Nilges, N., Pannu, N. S., Read, R. J., Rice, L. M., Simonson, T., and Warren, G. L. (1998) *Acta Crystallogr. Sect. D Biol. Crystallogr.* **54,** 905–921
24. Jones, T. A., Zou, J. Y., Cowan, S. W., and Kjeldgaard, M. (1991) *Acta Crystallogr. Sect. A Found. Crystallogr.* **47,** 110–119
25. Schuttelkopf, A. W., and van Aalten, D. M. (2004) *Acta Crystallogr. Sect. D Biol. Crystallogr.* **60,** 1355–1363
26. Laskowski, R. A., MacArthur, M. W., Moss, D. S., and Thornton, J. M. (1993) *J. Appl. Crystallogr.* **26,** 283–290
27. DeLano, W. L. (2004) *The PyMOL Molecular Graphics System*, DeLano Scientific LLC, San Carlos, CA
28. Munger, C. (2002) *Enzymatic mechanism of the fructose 1,6-bisphosphate aldolase from rabbit muscle: Role study of serines 271 and 300 from the active site*, Master's thesis, Université de Montréal, Qc, Canada
29. Ginsburg, A., and Mehler, A. H. (1966) *Biochemistry* **5,** 2623–2634
30. Morris, A. J., and Tolan, D. R. (1994) *Biochemistry* **33,** 12291–12297
31. Hannaert, V., Bringaud, F., Opperdoes, F. R., and Michels, P. A. (2003) *Kinetoplastid. Biol. Dis.* **2,** 11–41
32. Cassidy, C. S., Lin, J., and Frey, P. A. (1997) *Biochemistry* **36,** 4576–4584
33. Iyengar, R., and Rose, I. A. (1981) *Biochemistry* **20,** 1223–1229
34. Richard, J. P. (1984) *J. Am. Chem. Soc.* **106,** 4926–4936
35. Rios, A., Amyes, T. L., and Richard, J. P. (2000) *J. Am. Chem. Soc.* **122,** 9373–9385
36. Rios, A., Crugeiras, J., Amyes, T. L., and Richard, J. P. (2001) *J. Am. Chem. Soc.* **123,** 7949–7950
37. Richard, J. P., and Amyes, T. L. (2001) *Curr. Opin. Chem. Biol.* **5,** 626–633
38. Maurady, A., Zdanov, A., de Moissac, D., Beaudry, D., and Sygusch, J. (2002) *J. Biol. Chem.* **277,** 9474–9483
39. Grazi, E., and Trombetta, G. (1974) *Biochim. Biophys. Acta* **364,** 120–127
40. Grazi, E., Sivieri-Pecorari, C., Gagliano, R., and Trombetta, G. (1973) *Biochemistry* **12,** 2583–2590
41. Periana, R. A., Motur-Degrood, R., Chiang, Y., and Hupe, D. J. (1980) *J. Am. Chem. Soc.* **102,** 3923–3927
42. Drechsler, E. R., Boyer, P. D., and Kowalsky, A. G. (1959) *J. Biol. Chem.* **234,** 2627–2634
43. Rutter, W. J., Richards, O. C., and Woodfin, B. M. (1961) *J. Biol. Chem.* **236,** 3193–3197
44. Rose, I. A., and O'Connell, E. L. (1969) *J. Biol. Chem.* **244,** 126–134
45. Venkataraman, R., and Racker, E. (1961) *J. Biol. Chem.* **236,** 1883–1886
46. Jia, J., Schorken, U., Lindqvist, Y., Sprenger, G. A., and Schneider, G. (1997) *Protein Sci.* **6,** 119–124
47. Siebers, B., Brinkmann, H., Dörr, C., Tjaden, B., Lilie, H., van der Oost, J., and Verhees, C. H. (2001) *J. Biol. Chem.* **276,** 28710–28718

# Stereospecific Proton Transfer by a Mobile Catalyst in Mammalian Fructose-1,6-bisphosphate Aldolase

Miguel St-Jean and Jurgen Sygusch

*J. Biol. Chem. 2007, 282:31028-31037.*
*doi: 10.1074/jbc.M704968200 originally published online August 29, 2007*

---